Controlling Length of Gold Nanowires with Large-Scale: X-ray Absorption Spectroscopy Approaches to the Growth Process

Hao Ming Chen,[†] Ru-Shi Liu,*[,†] Kiyotaka Asakura,[‡] Ling-Yun Jang,[§] and Jyh-Fu Lee[§]

Department of Chemistry, National Taiwan University, Taipei 106, Taiwan, Catalysis Research Center, Hokkaido University, Sapporo, Japan, and National Synchrotron Radiation Research Center, Hsinchu 300, Taiwan

Received: September 3, 2007; In Final Form: October 11, 2007

By utilizing the X-ray absorption approach, the gold ions evolving from the Au−Cl complex to Au rods have been elucidated. The theoretical simulation of X-ray absorption spectra further revealed the evolution of gold and concluded that ultrafine small clusters of gold (Au_{13}) formed after a reducing agent was added to the growth solution. A redesigned seed-assisted growth method, a serial addition of growth solution, was employed to achieve the goal of the consecutive support of gold. The development approach was found to successfully fabricate 1D gold nanorods/wires with a tunable size from 50 nm to 1.7 μm.

Introduction

The synthesis of metal nanoparticles has been a research issue for decades owing to their widespread use in electronics, photonics, catalysis, information storage, optical sensing, biological labeling, imaging, and surface-enhanced Raman scattering.[1−5] The properties of metal nanoparticles are dependent on their size, shape, composition, and crystallinity.[6] By properly controlling these parameters, it is possible to tailor their properties for various applications. The intense study devoted to metal nanoparticles is motivated mainly by their extremely interesting optical properties. The wavelength of the plasmon resonance depends on several parameters, among which particle size and shape, surface charge, and the nature of the environment are probably the most important.[7] As a result, shape control has received considerable attention because it allows one to fine-tune the properties with greater versatility.[8] In this regard, gold and/or silver nanostructures have attracted substantial interest because of their size- and shape-dependent optical properties. Specially, one-dimensional (1D) gold nanostructures have received great attention owing to their biological applications[9] and size-dependent optical properties that can be tuned by varying the aspect ratio of the rods.[7,10] Several synthetic methods exist for preparing gold nanorods, such as electrochemical deposition on hard templates,[11] electrochemical synthesis in solution,[10a] photochemical methods,[12] and the seed-mediated method.[13] In addition to the hard template approach (porous membranes), most of the other methods rely on the use of a surfactant as a soft template in the experimental solution. Cationic ammonium surfactants have been used as soft template and directing agent in the synthesis of 1D gold nanorods in aqueous solutions; the most widely used surfactant is cetyltrimethylammonium bromide (CTAB). CTAB surfactants adsorb to gold nanorods in a bilayer fashion with the trimethylammonium headgroups in the first monolayer facing the gold surface.[14] Preferential adsorption of CTAB to the different crystal faces of gold leads to the inhibition of growth along the long axis of the rods, thereby enhancing growth at the ends of rods. The growth mechanism of gold nanorods in the presence of CTAB has been investigated extensively considering the influence of pH value,[15] nature of the seed,[16] heat treatment,[17] and so on. However, most of the studies in the synthesis of gold nanorods have focused on the roles of CTAB;[18] little attention has been given to the evolution of gold during the reaction and growth. The lack of information on the processes occurring in the reaction vessel during the growth of gold hinders the development of predictable shape-control schemes.

It is vitally important to study the fundamentals of gold growth because the understanding of this aspect will guide us to newer material design and a more sophisticated synthetic method. Although X-ray crystallography is extremely powerful as a structural probe, it provides only a description of the structure in the solid state. In contrast, most chemical reactions take place in solution. Reactive intermediates also are, by definition, difficult or impossible to crystallize. To accurately follow the reaction, it is essential to confirm that the crystallographic structure accurately represents the molecule of interest when it is in solution. One promising way to achieve this goal involves using X-ray absorption spectroscopy (XAS) here especially for the solution phase.[19a] The study of the extended X-ray absorption fine structure (EXAFS) has been particularly useful in providing local structural information about the noncrystalline,[19] and the X-ray absorption near-edge structure (XANES) can characterize the chemical bonding environment of the absorbing atoms and can be used to derive the effective oxidation state of the metal atoms.[20] In this report, utilization of XAS allows us to approach the growth of gold and propose a growth mechanism. On the basis of these principles and our results with gold 1D nanomaterials, we have been able to grow nanorods/wires with a continuous size of 50−1700 nm.

Experimental Section

Chemicals and Materials. Hydrogen tetrachloroaurate (III) hydrate, trisodium citrate dehydrate (99%), silver nitrate (99%), ascorbic acid (AA) (99%), and cetyltrimethylammonium bromide (CTAB) (99%) were obtained from Acros Organics and

* Author to whom correspondence should be addressed. E-mail: rsliu@ntu.edu.tw.
[†] National Taiwan University.
[‡] Hokkaido University.
[§] National Synchrotron Radiation Research Center.

10.1021/jp0770615 CCC: $37.00
Published on Web 11/29/2007

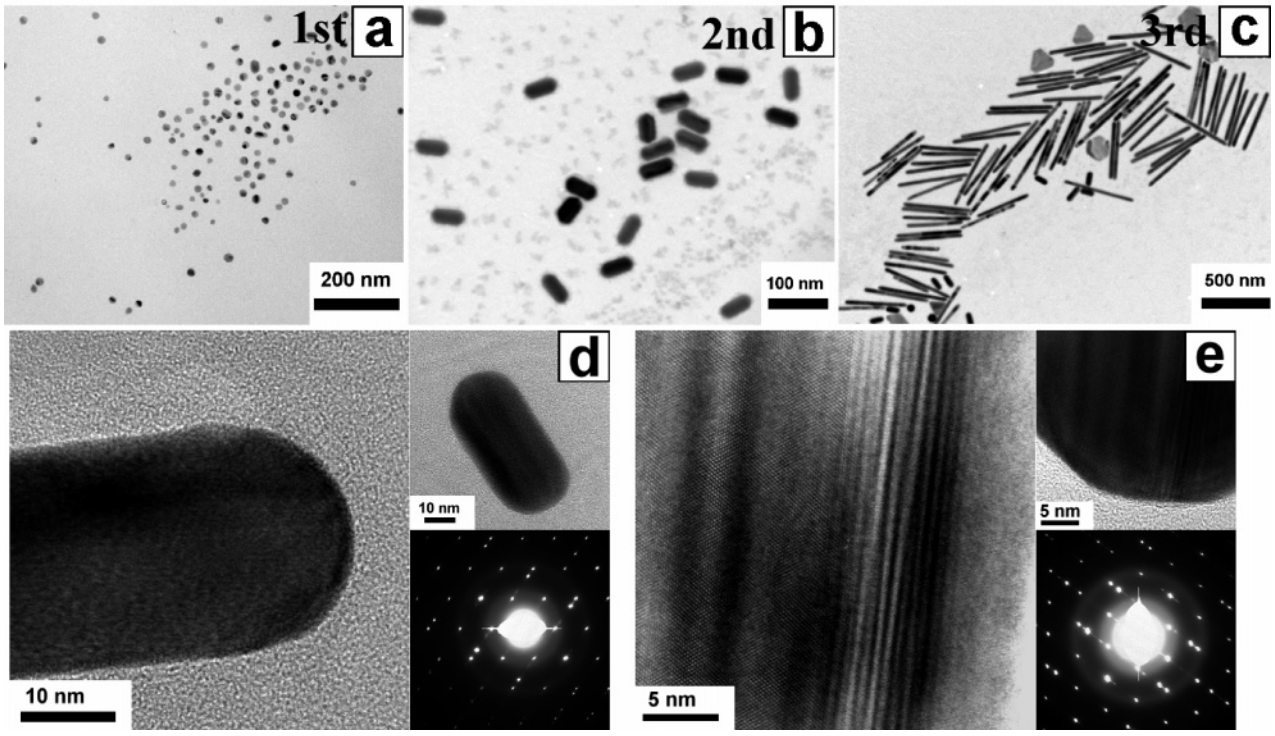

Figure 1. TEM images of gold resulting products after first growth addition (a), second growth addition (b), and third growth addition (c). (d and e) HRTEM images and SAED patterns corresponding to short (Figure 1b) and long (Figure 1c) gold nanorods.

used without further purification. The water used throughout this investigation was reagent-grade water, produced using a Milli-Q SP ultrapure-water purification system from Nihon Millipore Ltd., Tokyo.

Preparation of Gold Seeds. An aqueous 1% trisodium citrate solution (0.35 mL) was added into 10 mL of an aqueous 0.25 mM $HAuCl_4$ solution. After the solution was stirred for 3 min, 0.3 mL of an ice-cold, freshly prepared aqueous 0.01 M $NaBH_4$ solution was added, followed by stirring for 5 min. The seed solution was kept at room temperature for ~2 h and was used further.

Preparation of Gold Nanowires. CTAB (0.1 M) and 0.25 mM $HAuCl_4$ aqueous solution were prepared as the growth solution; the solution was stored at 27 °C throughout the experiment. Gold seeds (0.1 mL) were placed in a beaker. Three quantities (1, 10, and 100 mL) of growth solutions were mixed with 0.06 mL (first), 0.6 mL (second), and 6 mL (third) of freshly prepared ascorbic acid solution (10 mM), respectively. The growth solution became colorless after the ascorbic acid solution was added. These three colorless solutions were added to the gold seed solution step by step at intervals of 30 s.

Serial Addition of Growth Solution. CTAB (0.1 M) and 0.25 mM $HAuCl_4$ aqueous solution were prepared as the growth solution; the solution was stored at 27 °C throughout the experiment. First, 5 mL of growth solution was mixed with 0.3 mL of freshly prepared ascorbic acid solution (10 mM). Serial growth solutions (5 mL) were added to the seed solution (0.1 mL) at 30 s intervals. After the desired volume of growth solutions was added, the reaction mixture was kept for 24 h before subsequent analysis.

Characterization. The UV/vis spectra of the colloidal nanoparticle solution were obtained using a SHIMADZU UV-1700 spectrophotometer with a 1 cm quartz cell at room temperature. Transmission electron microscopy (TEM) was used to characterize the surface morphology of the samples. The TEM images were collected on a JEOL JEM-2010 electron microscope. The images of high-resolution transmission electron microscopy (HRTEM) and electron diffraction patterns were collected on a JEOL JEM-2100F electron microscope. The specimens were obtained by placing many drops of the colloidal solution onto a Formvar-covered copper grid and evaporating it in air at room temperature. Prior to specimen preparation, the colloidal solution was sonicated for 1 min to improve the dispersion of particles on the copper grid. A series of XAS measurements of the synthesized samples were made using synchrotron radiation at room temperature. Measurements were made at the Au L_3-edge (11918 eV) at room temperature.

XAS Data Analysis. The Wiggler-C beam line of the National Synchrotron Radiation Research Center (NSRRC), Taiwan, has been designed for such experiments. The back-scattering amplitude and phase shift functions for specific atom pairs were calculated ab initio using the FEFF8 code.[21] X-ray absorption data were analyzed following standard procedures, including preedge and postedge background subtraction, normalization with respect to edge height, Fourier transformation, and nonlinear least-squares curve fitting.[22] EXAFS analyses were carried out using an analysis package, "REX" or "REX2000", coded by Rigaku. The normalized k^3-weighted EXAFS spectra, $k^3x(k)$, were Fourier-transformed in the k range from 2.0 to 13.5 $Å^{-1}$ to reveal the contribution of each bond pair on the Fourier transform (FT) peak. The experimental Fourier-filtered spectra were obtained by performing an inverse Fourier transformation with a Hanning window function with r between 1.9 and 3.2 Å. The S_0^2 (amplitude reduction factor) value of the Au atoms was fixed at 0.85 to determine the structural parameters of each bond pair.

The results of simulations of gold atoms are based on the theoretical approach implemented in the relativistic, self-consistent FEFF8 code. The cluster size of the multiple-scattering calculation is specified by the FMS card and that for the self-consistent field calculations by the SCF card in the input

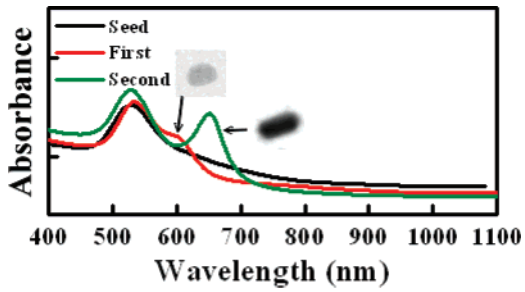

Figure 2. Extiction spectra of seeds, resulting products after first and second growth addition.

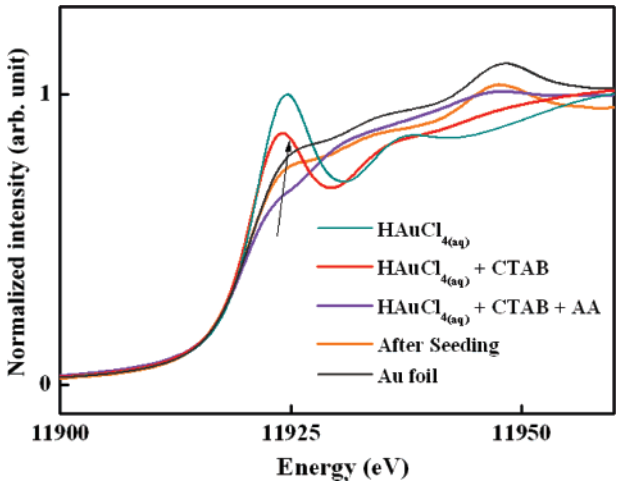

Figure 3. XANES spectra of Au L_3-edge for each reaction step.

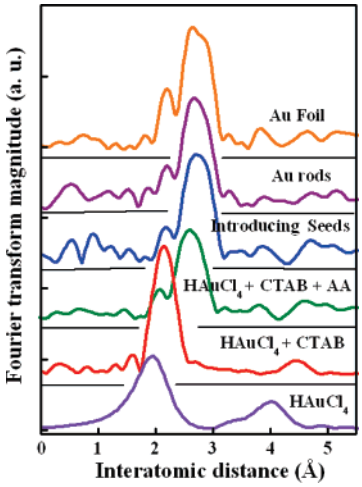

Figure 4. Fourier transforms of Au L_3-edge EXAFS spectra for each reaction stage.

TABLE 1: AuL_3-Edge EXAFS Structural Parameters of Each Reaction Stage, Au Rods, and Au Foil

sample	path	R (Å)	CN	σ (Å)	ΔE (eV)
$HAuCl_4$	Au−Cl	2.37 (3)	3.2 (5)	0.076 (5)	4.2 (7)
$HAuCl_4$ + CTAB	Au−Br	2.50 (5)	3.6 (6)	0.082 (4)	6.3 (6)
$HAuCl_4$ + CTAB + AA	Au−Au	2.80 (9)	5.1 (6)	0.101 (7)	−3.3 (7)
introducing seeds	Au−Au	2.81 (6)	8.8 (4)	0.089(6)	3.2 (7)
Au rods	Au−Au	2.85 (4)	10.7 (5)	0.069 (5)	−1.2 (3)
Au foil	Au−Au	2.86 (3)	11.8 (4)	0.0045 (5)	1.0 (5)

file. Default values of other input options were used. The only nonstandard input to FEFF8 was the EXCHANGE card (EXCHANGE 0/1 0 0.25), indicating that the calculations are carried out using the Hedin−Lundqvist/Dirac−Hara plasmon-pole self-energy, without any shifts, and with some additional broadening (0.25 eV). These parameters usually agree better with experimental results. Hedin−Lundqvist background function was used for $HAuCl_4$ solution and mixture of $HAuCl_4$ and CTAB solution (molecular). Dirac−Hara background function was used for adding reductant (ascorbic acid) into the growth solution (solid).[23]

Results and Discussion

Addition Effect and Optical Properties. Figure 1a−c shows the TEM images of the resulting product. When the first addition of growth solution was added to the seed solution, spherical particles were the major product; only a few short nanorods were obtained owing to the small amount of growth solution available as a gold ion source (Figure 1a). When the second and third growth solution were used to grow the nanorods, the average lengths were found to be ∼59 nm and ∼570 nm, respectively. The gold nanorods were formed in high yield, together with a small percentage of rough nanoplates (Figure 1c). The nanorods are relatively uniform in both diameter and length. High-resolution TEM images (Figure 1d) of these shorter rods (second) show diffraction contrast along the growth axis of the nanorods, indicating that the structure is not single-crystalline. The structure is twinned along the long axis. Electron diffraction analysis confirmed the superposition of specific crystallographic zones corresponding to the <110> and <111> zones of the face-centered cubic structure. In the case of the third addition, results of selective area electron diffraction and HRTEM (Figure 1e) showed that nanorods (third) were isometric pentafold twinned around their growth axis, which was along the [110] direction. Each section was separated by (111) planes and each rod has 5 {100} side faces and 10 {111} end faces, which was consistent with previous study of nanorods prepared in CTAB medium.[24]

Because the nanostructure of gold is well known to exhibit distinctive SPR features that depend strongly on their shape and structure, the shape evolution of the product could be conveniently followed by the UV/vis spectroscopic method. Figure 2 shows the absorption spectra of nanorods prepared in present study. The surface plasmon absorption spectra of 1D gold nanostructures are usually characterized by two bands. The absorption band appearing at the shorter wavelength is attributed to the transverse band, and that appearing at a longer wavelength corresponds to the longitudinal band.[7] It can be seen that through increasing the additional volume of growth solution the longitudinal plasmon band red-shifts and its intensity increases. When the first addition of growth solution was added to the seeds, only a small shoulder was found, which shows that most of the resulting nanoparticles were spherical. As more growth solution was added, the extinction spectrum exhibited a two-band feature, which verified the formation of 1D nanostructures. Notably, optical properties of these short gold nanorods are very close to the trend predicted by discrete dipole approximation (DDA). Simulations of the absorption efficiency using the DDA method and taking into account the real shape of gold nanorods have been reported.[25] Its maximum position λ_{max} shifts to the red as the aspect ratio increases. Simulated data is obtained for the equation below:

$$\lambda_{max} = 96\ \mathrm{AR\ (aspect\ ratio)} + 418 \qquad (1)$$

Applying 2.4 (AR was obtained in this study) to eq 1 gives λ_{max} = 648 nm, which is very close to our observation (649 nm).

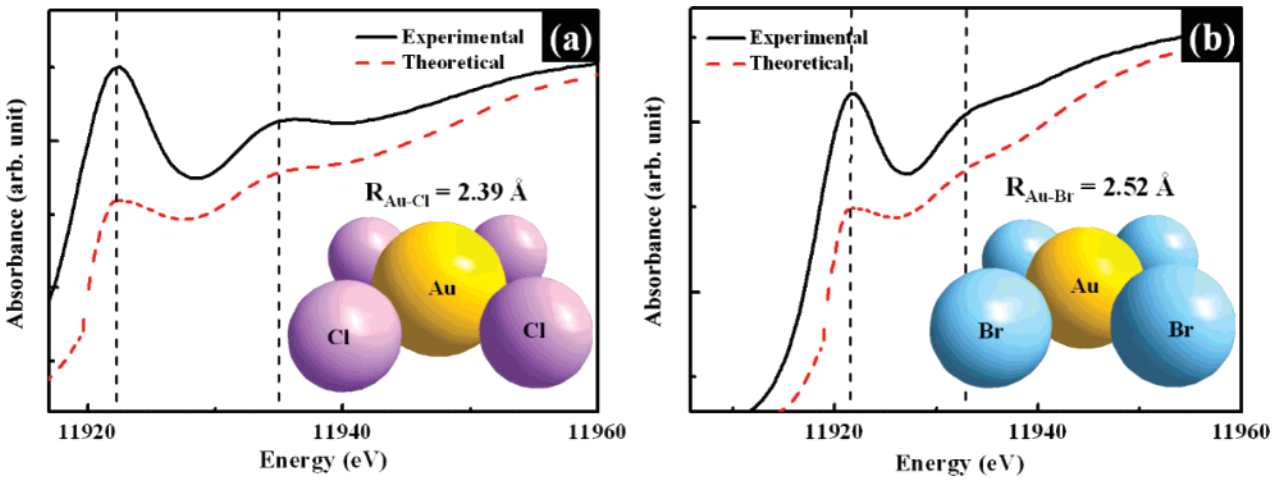

Figure 5. (a) Comparison between experimental spectrum and that calculated with FEFF for the Au−Cl complex. (b) Comparison between experimental spectrum and that calculated with FEFF for the Au−Br complex.

XANES Analysis of Gold throughout the Reaction. X-ray absorption spectroscopy experiments were performed to provide a better understanding of the oxidation state of gold nanoparticles throughout the reaction. Figure 3 plots the XANES of the Au L_3-edge throughout the experiment, which can distinguish the absorption spectra of gold during the reaction. The spectrum after CTAB was added to the precursor ($HAuCl_4$) has a similar structure, whereas the white line significantly decreased in intensity. The L_3-edge white line intensity depends on the electronic charge transfer between the absorbing atoms and ligands.[26] One should consider that chloride ions from $AuCl_4^-$ will (at least partially) exchange with bromide ions from CTAB because the bromide concentration is much higher than that of chloride. The interaction of the gold with the bromide has the effect of increasing the number of unoccupied d states of the gold. This result indicates a certain degree of electron transfer from bromide to gold, which elucidates the existence of the ligand exchange. Numerous studies have utilized the shape of the edge as a probe to determine the chemical state of the metal.[27] When ascorbic acid (as reducing agent) was added into the growth solution, the spectrum underwent a striking change and the white line intensity damped considerably. Although the position of the absorption edge in the K-edge was strongly dependent on the oxidation state of absorbing atoms, this effect usually was not operated in L_3-edge especially for 5d elements.[26] The expected absorption edge shifts are not readily observed in all cases because the actual edge is superposed to a varying extent by a prominent peak ($2p_{3/2}5d$ transition), which depends on the oxidation state of gold. From the formal electronic configuration for the gold, Au^0 ($5d^{10}6s^1$), Au^{1+} ($5d^{10}6s^0$), and Au^{3+} ($5d^86s^0$), it is supposed that only the Au^{3+} can exhibit the $2p_{3/2} \rightarrow 5d$ transition. Nevertheless, in an actual condition, the proximity between the Au 5d and 6s levels can cause the orbital mixing and the d-orbital vacancy even in Au^0 or Au^{1+} states, allowing the $2p_{3/2} \rightarrow 5d$ transition.[28] Notably, the intensity of this peak appears to increase with increasing unoccupied d densities of states.[28c,d] This decrease in intensity of the white line, as mentioned above, can be attributed to the fact that Au^{3+} ions were reduced to Au^0 and/or Au^{1+} by ascorbic acid. Nevertheless, we believe that most of Au^{3+} ions were reduced to Au^0 atoms because the stoichiometry of the reagents in the present synthesis is such that the amount of ascorbic acid is enough to reduce all of the gold salt in the solution. Theoretically, each ascorbic acid molecule loses two electrons upon oxidation,[17] and for reducing Au^{3+}, three electrons are needed per gold ion. Therefore, the ascorbic acid to gold salt ratio should be at least 1.5 to make the complete reduction of gold. We have used the ascorbic acid to gold salt ratio of ∼2.4, which would completely reduce all gold ions in the solution. When seeds were mixed with growth solution in which ascorbic acid had been added, the near edge structure was similar to that of gold foil while the intensity of solution after seeding was clearly lower than that of gold foil. This indicated that the resulting product had a structure similar to that of bulk gold after growth solution was added to the seeds.

EXAFS Analysis of Gold throughout the Reaction. Figure 4 shows the Fourier transforms (FT) of Au L_3-edge EXAFS spectra for each reaction stage. As aqua $HAuCl_4$ was mixed with CTAB, a strong peak appearing in the FT corresponded to the Au-complex change from ∼1.9 to ∼2.1 Å before phase correction, which indicated that the first shell around the Au^{3+} atoms was Br atoms instead of Cl atoms. After ascorbic acid (AA) was added, the Au^{3+} atoms were reduced to Au^0 and led the radius of Au atoms to increase. Thus, the peak appears at ∼2.6 Å before phase correction arising from the Au−Au scattering in ultrafine gold nanoparticles. The FT of small particles often gives the peak at a shorter distance, which also means that a somewhat structural contraction occurred in this stage. This can be attributed to core-level binding-energy shifts relative to the Fermi level.[29] On forming the metal, there is a flow of charge into the volume appropriate to the Wigner−Seitz cell, leading to a charge compression with the result that the binding energy is smaller in the bulk metal than in the free atoms.[30] For small clusters where a significant fraction of the atoms are located in surface sites, a net binding energy intermediate between the free atom and bulk metal is expected. Alternatively, the observed bond-length contraction with decreasing cluster size can also be explained by the aforementioned redistribution of charge.[31] In a surface, the number of nearest-neighbor atoms is significantly less in the bulk, which leads to a reduction in repulsive interactions between nonbonding electron pairs. A contraction of nearest-neighbor distance is the result, and therefore both EXAFS and XANES verify the formation of ultrafine nanoclusters. As seed was added, a strong peak at ∼2.7 Å before phase correction appearing in the FT arising from scattering of Au atoms. Seed particles are believed to provide active sites for subsequent crystal growth; gold atoms suspended in solution begin to grow and deposit on the surface of seeds. After a sufficient period of growth, this epitaxial deposition will lead to the growth of gold seeds. The peak corresponding to the scattering of the Au−Au path became sharper than the addition of ascorbic acid, which suggests the

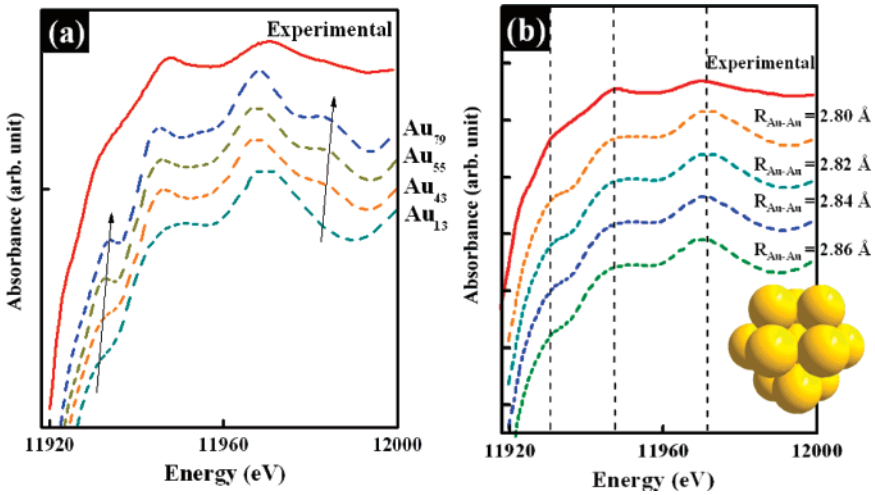

Figure 6. (a) Size effect on the XANES spectra for Au_{13}, Au_{43}, Au_{55}, and Au_{78}. (b) XANES spectra as calculated with FEFF for a 13-atom cluster of gold with different interatomic distances. (R_{Au-Au} = 2.80, 2.82, 2.84, and 2.86 Å).

growth of gold nanocrystals. Structural parameters for each spectrum are obtained by EXAFS refinement (Table 1). The evolution of the first metal−metal distance, which decreases from 2.86 Å for Au foil and 2.85 Å for Au rods to 2.81 Å for introducing seeds, confirms the contraction of the first coordination shell distance. The clusters after adding ascorbic acid feature an intermediate *R* value at 2.79 Å, the Au−Au bond distance could be correlated to some extent with the size of particles. When a highly disordered system is analyzed by the usual EXAFS analysis, the coordination number is much reduced and the interatomic distance appears shorter than the real value. In fact, the apparent bond length derived from EXAFS gets shorter with raising temperature owing to the large thermal disorder although it should be elongated by thermal expansion.[22]

In the case of adding AA, a low coordination number (5.1) was due to its smaller size, this value is slightly lower than expected (ideally 5.5) for an Au_{13} cluster. As seeds were introduced into the growth system, the coordination number increased to 8.8 owing to the presence of seed particles and an epitaxial growth of gold. The ultrafine clusters (smaller than 1 nm) grew upon the surfaces of seeds, which led to the increase of coordination number. With the progressive growth of gold, growing from small nanocrystals (8.8) to nanorods (10.7), the coordination number increased further. The coordination numbers of both the nanocrystals and nanorods were substantially lower than those for bulk Au, as expected from the presence of a high proportion of surface atoms as is the nature of nanomaterials. The Debye−Waller factor (σ) corresponding to the first shell showed a great variation according to the situation of the sample, from 0.045 Å for Au foil to 0.069 Å for Au rods prepared in the present method and up to 0.101 Å for the clusters formed after adding AA. The case of the sample after seeds have been introduced has a lower coordination number and higher Debye−Waller factor than that of Au nanorods. One interpretation of the low coordination number and high Debye−Waller factor could be that the Au atoms are looser in the as-formed gold clusters than those in gold nanorods. It is reasonable to believe that gold nanorods have better crystallinity than the as-formed gold clusters, for instance, the relative absence of disorder in the form of stacking, as is usually found for small metal cluster sizes.

Theoretical Simulation of XANES. To demonstrate the structure and geometry of gold during the reaction more accurately, we manipulated a theoretical simulation study of XANES. In the present study, we have used theoretical simulations based on the ab inito relativistic, self-consistent code FEFF8 to show that XANES can provide considerable insight into the morphology of gold.[5] This code is based on a full multiple scattering, real-space Green's function formalism. These include the study of small Pt clusters, Cu clusters, Cu/Mn clusters, and Cu/Pd clusters.[32] Figure 5a shows the experimental data of $HAuCl_4$ and theoretical simulation spectrum based on the model in which $AuCl_4^-$ has a square planar structure (D_{4h}). In FEFF8 code, the cluster size of the multiple-scattering calculation is specified by the FMS card (i.e., FMS 3.0) and that for the self-consistent field calculations by the SCF card in the in the input file (SCF 3.0), only the first shell was taken into consideration. It clearly elucidates that the theoretical simulation spectrum matched well with the experimental one. Our computed value was found to be ∼2.39 Å; this is slightly longer than those obtained from the quantum chemical calculated one (2.36 Å).[33] This is because $AuCl_4^-$ in this study was not in the solid phase, rather the molecular phase. Gold ions may be surrounded by solvent molecules (e.g., H_2O), which leads to the weakening of the overlap between orbitals of gold and those of chloride and makes the Au−Cl bonds longer. Figure 5b shows the experimental data of a mixture of $HAuCl_4$ and CTAB and theoretical simulation spectrum based on the model in which $AuBr_4^-$ has a square planar structure (D_{4h}). As CTAB was added into the $HAuCl_4$ solution, a ligand exchange occurred and simultaneously chloride ions were replaced with bromide ions. We operated the simulation through using a model similar to that of the operation in $AuCl_4^-$ molecules, scattering atoms (change from Cl to Br) and interatomic distance were optimized. Note that the calculation results demonstrated that the bond length for a Au−Br bond was ∼2.52 Å; this increase in bond length (0.13 Å) corresponded to the difference in atomic radius between chloride and bromide (0.12 Å).[34] As a result, bromide at certainly high concentration (100 times higher than that of chloride) should strongly affect the following course of reaction and growth of gold.

Figure 6 shows the experimental data of adding ascorbic acid and the theoretical simulation spectrum based on the model considering gold atoms have faced-centered cubic structure ($Fm\bar{3}m$). Nevertheless, there should be no negligible effects owing to factors in the structure of the clusters: (a) cluster size and (b) lattice contraction. To investigate cluster size effects on XANES spectra, several calculations were performed with

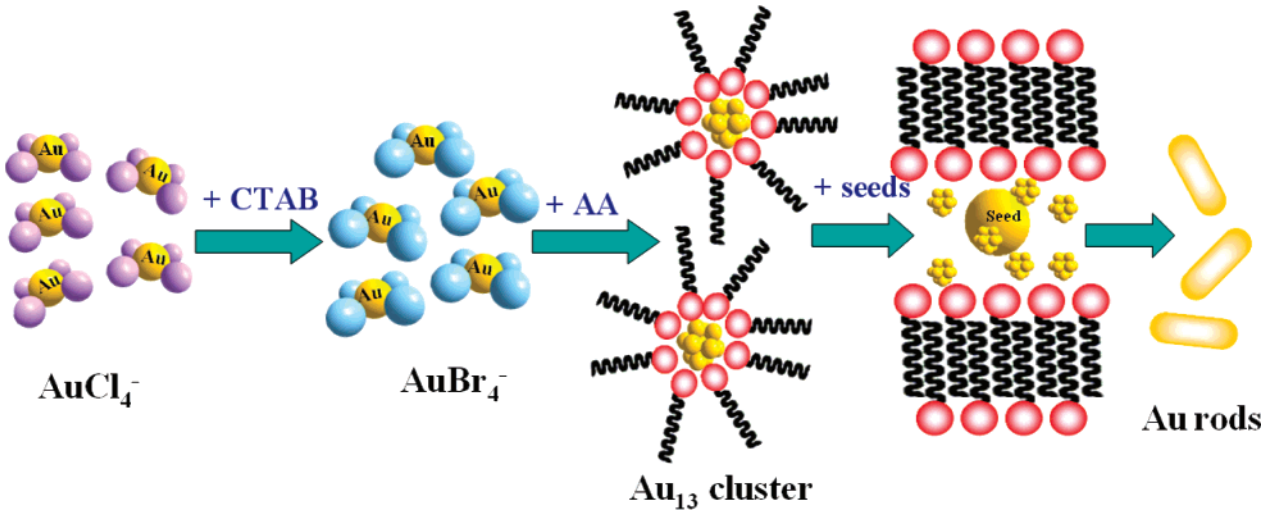

Figure 7. Evolution of gold at an early stage.

raising number of atoms. As shown in Figure 6a, the intensity of the white line varies slowly with the size of the cluster (indicated by an arrow). This is a direct consequence of the existence of inequivalent sites in small clusters, which concludes that a size effect is directly observable on the white line. Most interestingly, the intensity of the white line increased from adding of ascorbic acid to gold foil (as indicated by an arrow in Figure 3); it is consistent with the evolution of the cluster size effect generated by theoretical simulation. Earlier, Lytle had shown that a small white line exists at the Au L_3-edge in accord with the band calculation of Mattheiss et al., who showed that there are unoccupied density states of $d_{5/2}$ and $d_{3/2}$ character in the vicinity of the Fermi level owing to some level of s-p-d hybridization.[27] Moreover, we have to point out that the simulation spectra exhibit another feature: the presence an additional peak located at about 11980 eV, which arises in intensity with increasing cluster size. Thus, all simulation spectra differ from those of the experiment except the simulation spectrum of Au_{13} displays a feature similar to the experimental results. At this step of the numerical simulation, we have to emphasize the ultrafine small clusters presented at this stage.

To evaluate the modifications coming from a slight variation of the interatomic distance, we have also performed a set of calculations for 13-atom clusters of gold with different Au−Au interatomic distances. As shown in Figure 6b, it is clear that the position of the resonance peaks varied slightly with the change of Au−Au bond length. A shift toward higher energies can be attributed to a smaller interatomic distance. Our results for the effects of interatomic distance in XANES is in reasonable agreement both in amplitude and relative splitting with that of a simulation with $R_{Au-Au} = 2.82$ Å, implying the occurrence of structural contraction. This lattice contraction in small particles has been reported, which usually takes place in nanomaterials.[35] Consequently, the XANES features cannot be explained only in terms of cluster size but the interatomic distance must be taken into account. Nonetheless, there are clear numerical trends in the XANES analysis, which give semiquantitative insight into the design of these gold cluster materials. Simulation of XANES for gold provides clear and accurate evidence to verify the presence of Au_{13} clusters with structural contraction.

According to the above observation, we summarized the evolution of gold as shown in Figure 7. After $HAuCl_4$ solution was mixed with CTAB as surfactant, chloride ions were replaced by bromide ions to form a complex ($AuBr_4^-$) with gold ions (Au^{3+}), which means that ligand-exchange occurred. Because ascorbic acid (AA) as a reducing agent was added into the $AuBr_4^-$ solution, the majority of gold ions (Au^{3+}) were reduced to Au^0 atoms and aggregated to form Au_{13} clusters. Additionally, surfactant (CTAB) acted as a stabilizer to prevent the Au_{13} clusters from further growth. As a result, the Au_{13} clusters can stably maintain this situation for a period as a result of the lack of color in the solution at this stage. Because the scattering cross section for these ultrasmall gold clusters (below 1 nm) is extremely small, the well-known surface plasmon resonance (SPR) absorption for gold nanoclusters in the UV/vis region could not be observed.[36] After introducing the seeds into the reaction system, these Au_{13} clusters formed after adding AA grew upon the surfaces of seeds, which indicated that an epitaxial growth is present in this system. An "autocatalytic growth mechanism" may be operated here to explain this observation; the presence of nanoparticles as seeds significantly enhances the growth steps rather than the nucleation steps.[37] At once, the surfactant acts as a growth director to serve a one-dimensional environment for the growth of gold because of the rodlike micelles formed by the surfactant. The hydrophobic tail of CTAB interdigitates to make a bilayer on the rods, with the cationic headgroup of the first monolayer facing the gold surface.[10b] As a consequence, an anisotropic growth takes place and 1D gold nanorods were prepared under these conditions.

Length Control of Rods/Wires. Because the growth of the seed particles to rod-shaped particles is terminated upon depletion of the gold atoms supply of the solution, we believe the fact that the length of nanorods can be prolonged further if the growth of gold is not terminated. The synthesis of gold nanowires in a wet chemical approach with size above microscale has not yet been reported even though silver nanowires on a micrometer scale have been fabricated.[2b,13b] We, according to the above observation in this study, redesigned the seed-mediated growth method. A serial addition of growth solution was employed to achieve the goal of supporting the gold continuously. The rod mixtures were then grown by serial addition of growth solution into the existing seed solution in the presence of reducing agent (ascorbic acid). Through TEM studies and statistical analysis, we have shown that the length and width of gold nanorods/wires increase gradually with increasing volume of growth solution (Figure 8). The average length and width of the product after adding 10 mL of growth solution were 58.1 ± 9.2 nm and 25.1 ± 0.9 nm, respectively. When 1200 mL of growth solution was used to grow the 1D gold nanomaterials, the length of gold rods extended to about 1700 nm (aspect ratio ~ 35). Moreover, we divided the growth

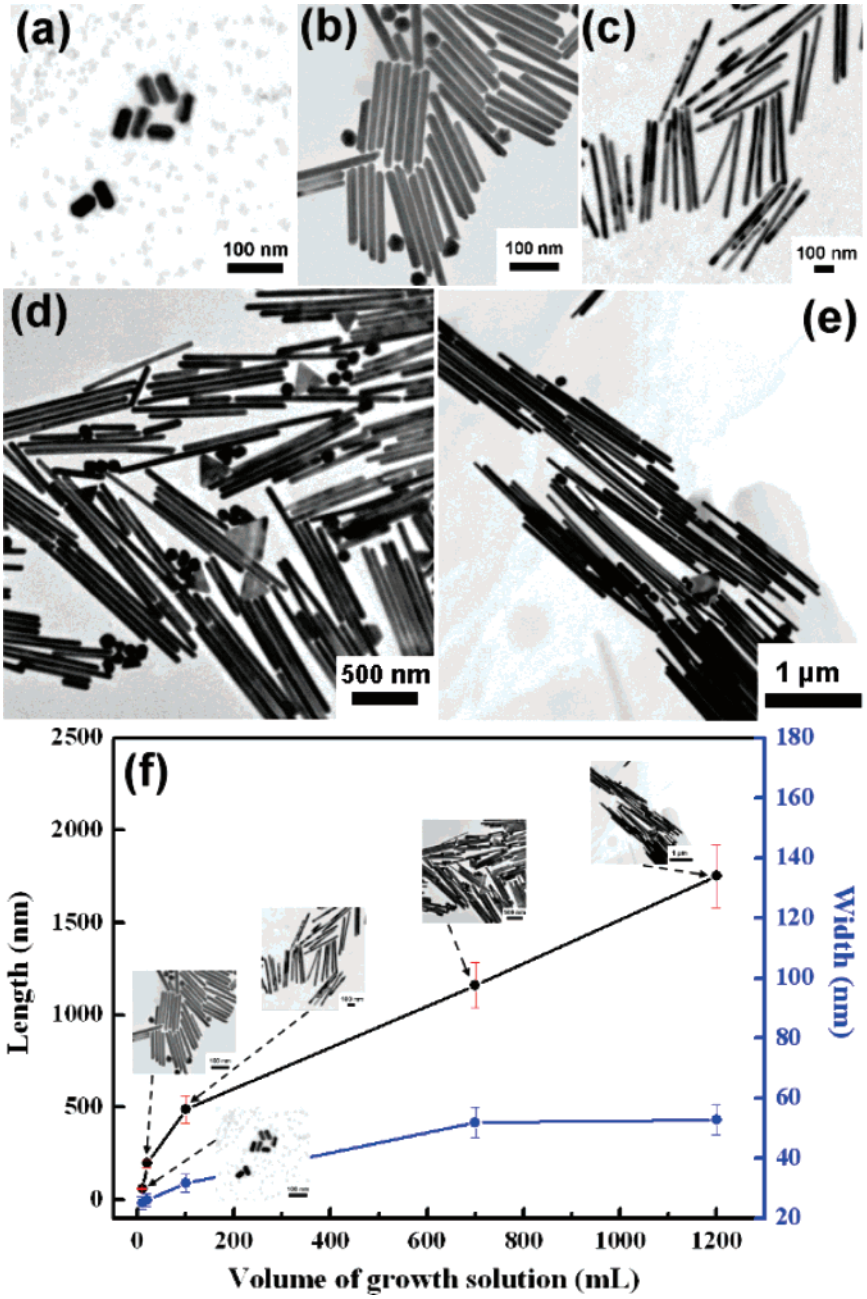

Figure 8. TEM images of resulting products after addition of 10 mL growth solution (a), 20 mL growth solution (b), 100 mL growth solution (c), 700 mL growth solution (d), and 1200 mL growth solution (e). Plot showing the dependence of the length and width on the volume of growth solution; the insets show TEM images of samples synthesized under the corresponding condition (f).

into two regions: (a) small amount of addition (from 10 to 100 mL) and (b) large amount of addition (from 100 to 1200 mL). In the case of length, the slope (nm/mL) of regions a and b from linear-regression analysis give 4.78 and 1.14, respectively. In the case of width, the slope (nm/mL) of regions a and b from linear-regression analysis give 0.081 and 0.019, respectively. The growth ratio between longitudinal and transverse axes can be defined as

$$\text{growth}^{\text{longitudinal/transverse}} = \frac{4.78}{0.081} \sim 59 \qquad \text{region a}$$

$$\text{growth}^{\text{longitudinal/transverse}} = \frac{1.14}{0.019} \sim 60 \qquad \text{region b}$$

This demonstrates that the growth rate between the longitudinal and transverse direction remained constant even if a large amount of growth solution was introduced into the reaction system to grow the gold 1D nanomaterials, which means that this novel approach can be extended to large scale easily. As a consequence, 1D gold nanorods/wires with desired lengths have been fabricated successfully via this method. To our knowledge, this is first example of high-yield gold nanowires with micrscale by means of a wet chemical synthesis.[10b,10c]

Conclusions

The present work has clearly established that gold ions evolved from the Au−Cl complex to Au rods through using the X-ray absorption approach. The theoretical simulation of X-ray absorption spectra further revealed that evolution of gold, ultrafine small clusters (Au_{13}) presented after reducing agent (ascorbic acid) was added to growth solution. XAS results allow the growth of gold and guide a proper scheme about the growth process. A serial addition of growth solution was employed to keep the supporting of gold, and 1D gold nanorods/wires with

tunable size up to microscale have been prepared successfully. Although the present work was focused on gold and CTAB, we believe that this new strategy can also be extended to other noble metals. We anticipate that continuous supply of metal atoms may provide a generic route to the synthesis of metal nanocrystals with controllable shapes, in high yields, and in large quantities.

Acknowledgment. We thank the National Science Council of the Republic of China, Taiwan for financially supporting this research under Contract No. NSC 95-2113-M-002-009.

Supporting Information Available: Best fitted EXAFS Au L_3-edge spectra of each reaction step (S1). This material is available free of charge via the Internet at http://pubs.acs.org.

References and Notes

(1) Electronics and photonics: (a) El-Sayed, M. A. *Acc. Chem. Res.* **2001**, *34*, 257. (b) Chen, S.; Yang, Y. *J. Am. Chem. Soc.* **2002**, *124*, 5280.

(2) Catalysis: (a) Lewis, L. N. *Chem. Rev.* **1993**, *93*, 2693. (b) Chen, M. S.; Goodman, D. W. *Science* **2004**, *306*, 252. (c) Valden, M.; Lai, X.; Goodman, D. W. *Science* **1998**, *281*, 1647. (d) Sinha, A. K.; Seelan, S.; Tsubota, S.; Haruta, M. *Angew. Chem., Int. Ed.* **2004**, *43*, 1546. (e) Kim, S. W.; Kim, M.; Lee, W. Y.; Hyeon, T. *J. Am. Chem. Soc.* **2002**, *124*, 7642. (f) Zhou, S.; Mcllwrath, K.; Jackson, G.; Eichhorn, B. *J. Am. Chem. Soc.* **2006**, *128*, 1780.

(3) Information storage: (a) Peyser, L. A.; Vinson, A. E.; Bartko, A. P.; Dickson, R. M. *Science* **2001**, *291*, 103. (b) Chen, H. M.; Liu, R.-S.; Li, H.; Zeng, H. C. *Angew. Chem., Int. Ed.* **2006**, *45*, 2713.

(4) Optical sensing, biological labeling, and imaging: (a) Kamat, P. V. *J. Phys. Chem. B* **2002**, *106*, 7729. (b) Park, S.-J.; Taton, T. A.; Mirkin, C. A. *Science* **2002**, *295*, 1503. (c) Charles Cao, Y. W.; Jin, R.; Mirkin, C. A. *Science* **2002**, *297*, 1536. (d) Rosi, N. L.; Giljohann, D. A.; Thaxton, C. S.; Lytton-Jean, A. K. R.; Han, M. S.; Mirkin, C. A. *Science* **2006**, *312*, 1027. (f) Elghanian, R.; Storhoff, J. J.; Mucic, R. C.; Letsinger, R. L.; Mirkin, C. A. *Science* **1997**, *277*, 1078. (g) Taton, T. A.; Mirkin, C. A.; Letsinger, R. L. *Science* **2000**, *289*, 1757.

(5) SERS: (a) Nie, S.; Emory, S. R. *Science* **1997**, *275*, 1102. (b) Tessier, P. M.; Velev, O. D.; Kalambur, A. T.; Rabolt, J. F.; Lenhoff, A. M.; Kaler, E. W. *J. Am. Chem. Soc.* **2000**, *122*, 9554.

(6) Kreibig, U.; Vollmer, M. *Optical Properties of Metal Clusters*; Springer: New York, 1995.

(7) Kelly, K. L.; Coronado, E.; Zhao, L. L.; Schatz, G. C. *J. Phys. Chem. B* **2003**, *107*, 668.

(8) (a) Wiley, B.; Sun, Y.; Mayers, B.; Xia, Y. *Chem.—Eur. J.* **2005**, *11*, 454. (b) Jin, R.; Cao, Y. C.; Hao, E.; Metraux, G. S.; Schatz, G. C.; Mirkin, C. A. *Nature* **2003**, *425*, 487. (c) Jin, R.; Cao, Y.; Mirkin, C. A.; Kelly, K. L.; Schatz, G. C.; Zheng, J. G. *Science* **2001**, *294*, 1901. (d) Sun, Y.; Wiley, B.; Li, Z.-Y.; Xia, Y. *J. Am. Chem. Soc.* **2004**, *126*, 9399. (e) Kim, F.; Connor, S.; Song, H.; Kuykendall, T.; Yang, P. *Angew. Chem., Int. Ed.* **2004**, *43*, 3673. (f) Ahmadi, T. S.; Wang, Z. L.; Green, T. C.; Henglein, A.; El-Sayed, M. A. *Science* **1996**, *272*, 1924. (g) Sun, Y.; Xia, Y. *Science* **2002**, *298*, 2176. (h) Chen, S.; Wang, Z. L.; Ballato, J.; Foulger, S. H.; Carroll, D. L. *J. Am. Chem. Soc.* **2003**, *125*, 16186.

(9) (a) Nikoobakht, B.; Wang, J.; El-Sayed, M. A. *Chem. Phys. Lett.* **2002**, *17*, 366. (b) Lee, K.-S.; El-Sayed, M. A. *J. Phys. Chem. B* **2006**, *110*, 19220. (c) Huang, X.; El-Sayed, I. H.; Qian, W.; El-Sayed, M. A. *J. Am. Chem. Soc.* **2006**, *128*, 2115.

(10) (a) Yu, Y.-Y.; Chang, S.-S.; Lee, C.-L.; Wang, C. R. C. *J. Phys. Chem. B* **1997**, *101*, 6661. (b) Murphy, C. J.; Sau, T. K.; Gole, A. M.; Orendorff, C. J.; Gao, J.; Gou, L.; Hunyadi, S. E.; Li, T. *J. Phys. Chem. B* **2005**, *109*, 13857. (c) Murphy, C. J.; Gole, A. M.; Hunyadi, S. E.; Orendorff, C. J. *Inorg. Chem.* **2006**, *45*, 7544.

(11) van der Zande, B. M.; Bohmer, M. B.; Fokkink, L. G. J.; Schonenberger, C. *J. Phys. Chem. B* **1997**, *101*, 852.

(12) (a) Esumi, K.; Matsuhisa, K.; Torigoe, K. *Langmuir* **1995**, *11*, 3285. (b) Kim, F.; Song, J. H.; Yang, P. *J. Am. Chem. Soc.* **2002**, *124*, 14316.

(13) (a) Jana, N. R.; Gearheart, L.; Murphy, C. J. *J. Phys. Chem. B* **2001**, *105*, 4065. (b) Murphy, C. J.; Jana, N. R. *Adv. Mater.* **2002**, *14*, 80. (c) Sau, T. K.; Murphy, C. J. *J. Am. Chem. Soc.* **2004**, *126*, 8648. (d) Chen, H. M.; Peng, H.-C.; Liu, R.-S.; Asakura, K.; Lee, C.-L.; Lee, J.-F.; Hu, S.-F. *J. Phys. Chem. B* **2005**, *109*, 19553.

(14) (a) Gao, J.; Bender, C. M.; Murphy, C. J. *Langmuir* **2003**, *19*, 9065. (b) Nikoobakht. B.; El-Sayed, M. A. *Chem. Mater.* **2003**, *15*, 1957.

(15) Busbee, B. D.; Obare, S. O.; Murphy, C. J. *Adv. Mater.* **2003**, *15*, 414.

(16) Gole, A.; Murphy, C. J. *Chem. Mater.* **2004**, *16*, 3633.

(17) Gou, L.; Murphy, C. J. *Chem. Mater.* **2005**, *17*, 3668.

(18) (a) Filankembo, A.; Pileni, M. P. *J. Phys. Chem. B* **2000**, *104*, 5865. (b) Tornblom, M.; Henriksson, U. *J. Phys. Chem. B* **1997**, *101*, 6028. (c) Reetz, M. T.; Helbig, W.; Quaiser, S. A.; Stimming, U.; Breuer, N.; Vogel, R. *Science* **1995**, *267*, 367. (d) Perez-Juste, J.; Liz-Marzan, L. M.; Carnie, S.; Chan, D. Y. C.; Mulvaney, P. *Adv. Funct. Mater.* **2004**, *14*, 571.

(19) (a) Penner-Hahn, J. E. *Coord. Chem. Rev.* **1999**, *190*, 1101. (b) Besenbacher, F.; Chorkendorff, I.; Clausen, B. S.; Hammer, B.; Molenbroek, A. M.; Norskov, J. K.; Stensgaard, I. *Science* **1998**, *279*, 1913. (c) Lee, W.-R.; Kim, M. G.; Choi, J.-R.; Park, J.-I.; Ko, S. J.; Oh, S. J.; Cheon, J. *J. Am. Chem. Soc.* **2005**, *127*, 16090. (d) Chen, H. M.; Liu, R.-S.; Asakura, K.; Lee, J.-F.; Jang, L.-Y.; Hu, S.-F. *J. Phys. Chem. B* **2006**, *110*, 19162. (e) Chen, H. M.; Hsin, C. F.; Liu, R.-S.; Lee, J.-F.; Jang, L.-Y. *J. Phys. Chem. C* **2007**, *111*, 5909.

(20) (a) Roth, C.; Benker, N.; Buhrmester, T.; Mazurek, M.; Loster, M.; Fuess, H.; Koningsberger, D. C.; Ramaker, D. E. *J. Am. Chem. Soc.* **2005**, *127*, 14607. (b) Zhang, J.; Sasaki, K.; Sutter, E.; Adzic, R. R. *Science* **2007**, *315*, 220. (c) Guzman, J.; Gates, B. C. *J. Am. Chem. Soc.* **2004**, *126*, 2672. (d) Immoos, C. E.; Sulc, F.; Farmer, P. J.; Czarnecki, K.; Bocian, D. F.; Levina, A.; Aitken, J. B.; Armstrong, R. S.; Lay, P. A. *J. Am. Chem. Soc.* **2004**, *127*, 814.

(21) Ankudinov, A. L.; Ravel, B.; Rehr, J. J.; Conradson, S. D. *Phys. Rev. B* **1998**, *58*, 7565.

(22) Iwasawa, Y. *X-ray Absorption Fine Structure for Catalysts and Surfaces*; World Scientific: Singapore, 1996.

(23) According to J. J. Rehr's suggestion about XANES simulation on website. 0 (Hedin−Lundqvist) is the default, recommended for solids. 1 (Dirac−Hara) sometimes is better than HL, especially in molecules.

(24) Johnson, C. J.; Dujardin, E.; Davis, S. A.; Murphy, C. J.; Mann, S. *J. Mater. Chem.* **2002**, *12*, 1765.

(25) Brioude, A.; Jiang, X. C.; Pileni, M. P. *J. Phys. Chem. B* **2005**, *109*, 13138.

(26) (a) Meitzner, G.; Via, G. H.; Lytle, F. W.; Sinfelt, J. H. *J. Phys. Chem.* **1992**, *96*, 4960. (b) Wong, J.; Lytle, F. W.; Messmer, R. P.; Maylotte, D. H. *Phys. Rev. B* **1984**, *30*, 5596.

(27) (a) Lytle, F. W.; Wei, P. S. P.; Greegor, R. B.; Via, G. H.; Sinfelt, J. H. *J. Chem. Phys.* **1979**, *70*, 4849. (b) Mansour, A. N.; Cook, J. W.; Sayers, D. E. *J. Phys. Chem.* **1984**, *88*, 2330. (c) Mattheiss, L. F.; Dietz, R. E. *Phys. Rev. B* **1980**, *22*, 1663. (d) Benfield, R. E.; Grandjean, D.; Kroll, M.; Pugin, R.; Sawitowski, T.; Schmid, G. *J. Phys. Chem. B* **2001**, *105*, 1961.

(28) (a) Pantelouris, A.; Kuper, G.; Hormes, J.; Feldmann, C.; Jansen, M. *J. Am. Chem. Soc.* **1995**, *117*, 11749. (b) Choy, J.-H.; Kim, Y. *J. Phys. Chem. B* **2003**, *107*, 3348. (c) Sham, T. K.; Yiu, Y. M.; Tan, K. H. *Phys. Rev. B* **1990**, *41*, 11881. (d) Sham, T. K.; Watson, R. E.; Perlman, M. L. *Phys. Rev. B* **1980**, *21*, 1457.

(29) Apai, G.; Hamilton, J. F.; Stohr, J.; Thompson, A. *Phys. Rev. Lett.* **1979**, *43*, 165.

(30) (a) Mason, M. G.; Gerenser, L. J.; Lee, S. T. *Phys. Rev. Lett.* **1977**, *39*, 288. (b) Connolly, J. W. *Phys. Rev.* **1967**, *159*, 415. (c) Watson, R. E.; Perlman, M. L.; Herbst, J. F. *Phys. Rev. B* **1976**, *13*, 2358.

(31) (a) Jones, R. O.; Jennings, P. J.; Painter, G. S. *Surf. Sci.* **1975**, *53*, 409. (b) Jennings, P. J.; Painter, G. S.; Jones, R. O. *Surf. Sci.* **1976**, *60*, 255.

(32) (a) Bazin, D.; Sayers, D.; Rehr, J. J.; Mottet, C. *J. Phys. Chem. B* **1997**, *101*, 5332. (b) Bazin, D.; Bensaddik, A.; Briois, V.; Sainctavit, Ph. *J. Phys. IV* **1996**, *6*, 481. (c) Greaves, G. N.; Durham, P. J.; Quinn, P. *Nature* **1981**, *294*, 139. (d) Ankudinov, A.; Rehr, J. J.; Low, J. J.; Bare, S. R. *J. Chem. Phys.* **2002**, *116*, 1911. (e) Bazin, D.; Rehr, J. J. *J. Phys. Chem. B* **2003**, *107*, 12398.

(33) Hargittai, M.; Schulz, A.; Reffy, B.; Kolonits, M. *J. Am. Chem. Soc.* **2001**, *123*, 1449.

(34) Pearson, W. B. *Crystal Chemistry and Physics of Metals and Alloys*; Wiley: New York, 1972.

(35) (a) Sinfelt, J. H.; Via, G. H.; Lytle, F. W. *J. Chem. Phys.* **1978**, *68*, 2009. (b) Solliard, C.; Flueli, M. *Surf. Sci.* **1985**, *156*, 487. (c) Duff, D. G.; Edwards, P. P.; Evans, J.; Gauntlett, J. T.; Jefferson, D. A.; Johnson, B. F. G.; Kirkland, A. I.; Smith, D. J. *Angew. Chem., Int. Ed.* **1989**, *28*, 590. (d) Hilsabeck, T. J.; Kabantsev, A. A.; Driscoll, C. F.; O'Neil, T. M. *Phys. Rev. Lett.* **2003**, *90*, 245002.

(36) (a) Kreibig, U.; Genzel, L. *Surf. Sci.* **1985**, *156*, 678. (b) Zheng, J.; Petty, J. T.; Dickson, R. M. *J. Am. Chem. Soc.* **2003**, *125*, 7780. (c) Crooks, R. M.; Zhao, M. Q.; Sun, L.; Chechik, V.; Yeung, L. K. *Acc. Chem. Res.* **2001**, *34*, 181.

(37) Jana, N. R.; Geartheart, L.; Murphy, C. J. *Chem. Mater.* **2001**, *13*, 2313.